Neutron halos in the excited states of ^{12}B

T. L. Belyaeva,[1] S. A. Goncharov,[2] A. S. Demyanova,[3] A. A. Ogloblin,[3] A. N. Danilov,[3] V. A. Maslov,[4] Yu. G. Sobolev,[4]
W. Trzaska,[5] S. V. Khlebnikov,[6] G. P. Tyurin,[6] N. Burtebaev,[7] D. Janseitov,[4,7] and E. Mukhamejanov[7,8]

[1]*Universidad Autónoma del Estado de México, C.P. 50000, Toluca, México*
[2]*Lomonosov Moscow State University, GSP-1, Leninskie Gory, Moscow 119991, Russia*
[3]*NRC Kurchatov Institute, Moscow 123182, Russia*
[4]*Flerov Laboratory for Nuclear Research, JINR, Dubna, Moscow Region 141980, Russia*
[5]*Department of Physics, University of Jyväskylä, P.O. Box 35, FI-40014 Jyväskylä, Finland*
[6]*V. G. Khlopin Radium Institute, St. Petersburg 194021, Russia*
[7]*Institute of Nuclear Physics, National Nuclear Center of Republic of Kazakhstan, Almaty 050032, Republic of Kazakhstan*
[8]*Al-Farabi Kazakh National University, Almaty 050040, Republic of Kazakhstan*

The differential cross sections of the ^{11}B(d, p)^{12}B reaction leading to formation of the 1^+ ground state and the 0.95-MeV 2^+, 1.67-MeV 2^-, 2.62-MeV 1^-, 2.72-MeV 0^+, and 3.39-MeV 3^- excited states of ^{12}B are measured at $E_d = 21.5$ MeV. The analysis of the data is carried out within the coupled-reaction-channels method for the direct neutron transfer and the Hauser-Feshbach formalism of the statistical compound-nucleus model. The spectroscopic factors, asymptotic normalization coefficients, and rms radii of the last neutron in all states studied are deduced. The existence of the neutron halos in the 1.67-MeV 2^- and 2.62-MeV 1^- states is found, consistent with the earlier published data. New information about the enlarged rms radii of the last neutron in the 2.72-MeV 0^+ (5.7 fm) and the unbound 3.389-MeV 3^- (5.9 fm) states of ^{12}B was obtained, resulting in the possible existence of neutron halo-like states in ^{12}B.

The discovery of neutron halos in some neutron-rich radioactive light nuclei located close to the neutron drip line [1,2] was one of the most remarkable discoveries in nuclear physics at the end of the 20th century. Nuclei possessing neutron halos were named exotic nuclei [3,4] because they are characterized by unusual properties. Neutron-halo nuclei are structured so that they are two-component objects: the intrinsic core with normal density is surrounded by a diffuse region with lower density containing only valence neutrons. As a result, the exotic nuclei possess dimensions much larger than those of "ordinary" nuclei with the same mass number. Among the most spectacular examples of such nuclei are the one-neutron-halo isotopes ^{11}Li and ^{11}Be, in the ground states of which the average distance between valence neutron and the center of the nuclear core can reach up to 7 fm and even 8 fm [5,6], that is, about three times larger than the rms radii of their stable isotopes. It should be particularly emphasized that the halo phenomenon has a universal character appearing not only in the ground states of exotic nuclei but in the excited states of normal nuclei [7–10]. Nevertheless, sufficiently precise and rigorous definitions of halos should be applicable irrespective of whether a halo is formed in the ground or excited state. Following Refs. [11–15] the halo state is characterized by (i) a large probability for finding a cluster component in the total many-body wave function and (ii) a large spatial extension implying that more than half of the probability should be in the classically forbidden region outside the outer classical turning point.

These are quite strict requirements, and it is important to answer the question of whether realistic halos satisfy to these criteria and how the halo features appear in less developed halos. The problem of halos in the excited states is related to the search for enlarged radii of nuclei in the short-lived excited states located close to and above the particle-emission threshold (the so-called size isomers). Considerable advances in this area have been made recently (see, e.g., Ref. [16] and references therein).

The ^{12}B nucleus is the only odd-odd nucleus in whose excited states neutron halos were detected [17]. The low-lying states of ^{12}B with negative parity are formed owing to the fact that the last neutron is brought into the $2s$ shell, and this fact contributes to the formation of a halo. The doublet of the 1.67-MeV 2^- and 2.62-MeV 1^- states possesses this structure. The states are located at 1.70 and 0.75 MeV, respectively, below the ^{12}B $+ n$ threshold. Liu *et al.* [17] were the first to report the observation of halos in these excited states of ^{12}B in (d, p) reactions on ^{11}B measured at 11.8 MeV, which they analyzed by the method of asymptotic normalization coefficients (ANC). The existence of neutron halos in these states is not only of certain astrophysical interest [18], but also has significance for the problem of appearance of halos as a whole. Application of the ANC theory [19–23] to peripheral reactions on light nuclei is especially adequate for determining the radii of halos [17,24]. In actual practice, the ANC theory is widely used to obtain spectroscopic and astrophysical information [25–29].

The 3.39-MeV 3^- state of ^{12}B located in the continuum spectrum (only 20 keV above the neutron emission threshold)

is of particular interest. The valence neutron in this state falls into the $1d$ shell. Note that the 3.39-MeV 3^- state is a sufficiently long-lived state, because its half-life is much greater than the characteristic nuclear time (an average flight time of the last neutron in its orbit in the nucleus), $\tau_{1/2} \gg \tau_{\rm fl}$. The ratio $\tau_{1/2}/\tau_{\rm fl}$ for this state is about 6×10^4 (the width of the state is $\Gamma = 3.1$ eV and the time of flight for a distance of about 6 fm by a neutron with energy 20 keV is approximately equal to 10^3 fm/c), which evidently satisfies the requirement to treat this state as a long-lived one. Note that the ratio $\tau_{1/2}/\tau_{\rm fl}$ for the 3.39-MeV 3^- state is substantially greater than that, for example, for the $1/2^+, 5/2^+, 3/2^+$ states belonging to the rotational bands of the ^{9}Be and ^{11}Be nuclei, in which neutron halos were revealed [16]. A factor that can prevent halo formation in the 3.39-MeV 3^- state is the high centrifugal barrier for the $l_n = 2$ orbital. An observation of the anomalously large neutron radius in this state comparable with those in the 1.67-MeV 2^- and 2.62-MeV 1^- states would indicate that the 3.39-MeV 3^- state can be a candidate for a neutron-halo state. Calculation of the neutron radius in the unbound 3.39-MeV 3^- state is possible, if we use the effective small positive binding energy of the valence neutron, taking into account the proximity of this state to the neutron emission threshold and its sufficiently long half-life.

Another important reason for interest in studying neutron halos in the excited states of ^{12}B is related to the fact that ^{12}B belongs to the isospin triplet including additionally the ^{12}C and ^{12}N nuclei. The measured ^{12}B and ^{12}N spectra are very similar and their low-lying levels correspond to the one-particle–one-hole shell-model configurations [30,31]. One can expect that excited states with halos can also appear in other nuclei of this triplet. In particular, a proton halo presumably can exist in the isobar-analog states of ^{12}N with spin-parities 1^- and 2^-. Unfortunately, the proton-emission threshold in ^{12}N is located only 0.60 MeV above the ground state (g.s.), which hinders application of the ANC method for direct calculation of the radii of ^{12}N in the excited states. The relationship of the ANCs for the g.s. of mirror nuclei was established in Refs. [32,33]. Thus the radii of ^{12}B in the halo states that will be presented in this paper are useful in estimating the radii of the nuclei with $A = 12$ determined by other methods. It should be mentioned in this connection that a possibility to apply the modified diffraction method (MDM) [34–36] for determining the radii of nuclei in the excited states by studying the charge-exchange $(^3\text{He}, t)$ reactions was recently proposed [37]. The first applications of MDM to the mirror states of ^{13}C and ^{13}N nuclei [37] have demonstrated the effectiveness of this new approach.

In this paper, new data for the ^{11}B$(d, p)^{12}$B reaction at deuteron energy 21.5 MeV are reported. The differential cross sections are measured for the g.s. and five excited states of ^{12}B. The data are analyzed by the statistical compound nucleus (CN) model and the coupled-reaction-channels (CRC) method for direct neutron transfer. The main goal of the work is to determine the radius of ^{12}B in the studied states by the ANC method. Particular attention is paid to the 3.389-MeV 3^- state to answer the question of whether there exists a neutron halo in this state formed by the valence neutron occupying the $l = 2$ orbital. The new data for other bound excited states
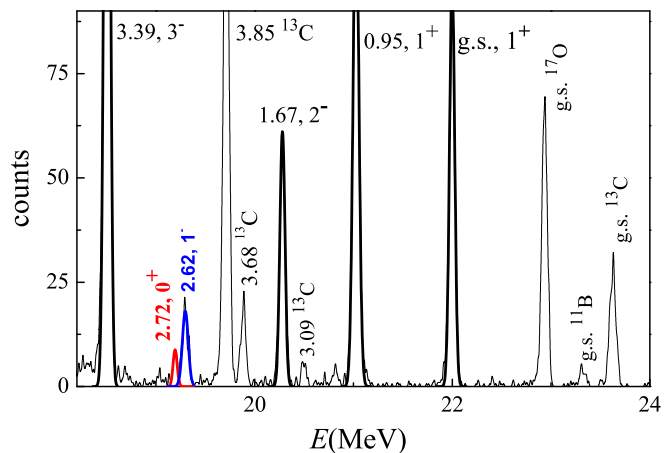
FIG. 1. A proton spectrum from the ^{11}B$(d, p)^{12}$B reaction at 18° (c.m.) with the excitation of ^{12}B states up to $E_x \approx 3.5$ MeV.

of ^{12}B, acquired at an appreciably higher energy than in Ref. [17], are also of undoubted interest. Preliminary results were previously reported in the conference paper Ref. [38], but only included a sketchy outline of the preliminary calculations. The present work presents complete measured data and a more thorough analysis using two different reaction models. It includes also a summary of the recent data concerning neutron halos in the excited states obtained by different methods.

The paper is organized as follows: Sec. II describes the experimental setup and the results of the measurements. The theoretical analysis within the Hauser-Feshbach formalism of the statistical CN model and the CRC method for direct neutron transfer is presented in Sec. III. The deduced spectroscopic factors (SFs), the ANCs, and the last neutron rms radii of ^{12}B in the excited states are presented in Sec. IV. In Sec. V, we discuss the results and compare the rms and halo radii of some light nuclei possessing neutron halos in the excited states. The conclusions are summarized in Sec. VI.

I. EXPERIMENTAL PROCEDURE AND RESULTS

The measurements were conducted at the University of Jyväskylä (Finland) using the K130 cyclotron to produce a deuteron beam at $E_{\rm d} = 21.5$ MeV. The 150 cm diameter Large Scattering Chamber was equipped with four ΔE-E detector telescopes, each containing two independent ΔE detectors and one common E detector. So each device allowed carrying out measurements at two angles. The measurements in c.m. angular range 10° were conducted in one exposure. The differential cross sections of deuteron elastic scattering and the (d, p) reaction on ^{11}B were measured in the c.m. angular range 5°–85°. A self-supported ^{11}B foil of 0.275 mg/cm^2 thickness was used as a target. The beam intensity was about 20 particle nA.

It should be mentioned that, before starting measurements, an additional beam monochromatization was done, which made it possible to diminish beam energy spreading up to three times and obtain a total energy resolution about 70 keV. In Fig. 1 a sample proton spectrum from the ^{11}B$(d, p)^{12}$B reaction at 18° (c.m.) showing the excitation of ^{12}B states up to
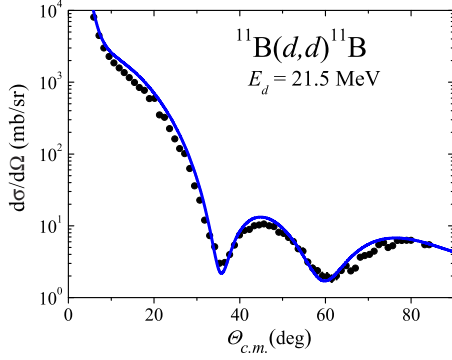
FIG. 2. Deuteron elastic-scattering CRC calculation (solid line) compared with the $d + {}^{11}$B elastic scattering cross section at 21.5 MeV measured in the present work (points).

$E_x \approx 3.5$ MeV is presented. Carbon (^{12}C) and oxygen (^{16}O) were the only impurities in the target, so peaks for excited states of ^{13}C and ^{17}O are also seen. All peaks are distinct and are well separated. The beam monochromatization made possible a separation of the neighboring 2.62-MeV 1^- and 2.72-MeV 0^+ states of ^{12}B.

A standard expansion method was employed to obtain cross sections: the spectrum peaks were fitted with a Gaussian shape. The peak positions and widths were fixed in accordance with the world-average values, and the area under the peak was the only free parameter.

Proton angular distribution for the g.s. and five first excited states of ^{12}B:, 0.95-MeV 2^+, 1.67-MeV 2^-, 2.62-MeV 1^-, 2.72-MeV 0^+, and 3.39-MeV 3^-, were measured. The resulting differential cross sections for the elastic deuteron scattering and the ^{11}B$(d, p)^{12}$B reaction are presented in Figs. 2–5.

II. THEORETICAL ANALYSIS

A. Elastic scattering analysis

The first step of the analysis includes choosing the reasonable optical potentials (OPs) to fit the experimental elastic-scattering angular distribution. The effective potentials are represented by the OPs of the standard form:

$$\mathbf{V}(r) = V_{\text{Coul}}(r) - V_0 f_0(r) + V_{\text{s.o.}} \left(\frac{\hbar}{m_\pi c} \right)^2 2(\mathbf{L} \cdot \mathbf{s})$$

$$\times \frac{1}{r} \frac{d}{dr} f_{\text{s.o.}}(r) - i \left[W - 4W_D \frac{d}{dr} \right] f_W(r), \quad (1)$$

$$f_i(r) = \left\{ 1 + \exp \left[\left(r - r_i A_T^{1/3} \right) \big/ a_i \right] \right\}^{-1}, \quad i = 0, \text{ s.o., and } W, \quad (2)$$

with the real, spin-orbital, and imaginary components, respectively. The Coulomb interaction is represented by the $V_{\text{Coul}}(r)$ potential of a uniformly charged sphere of radius $R_C = r_C A_T^{1/3}$.

Parameters of the OP used for the $d + {}^{11}$B channel at 21.5 MeV are chosen based on the global parametrization presented in Refs. [39,40] and taking into account the elastic
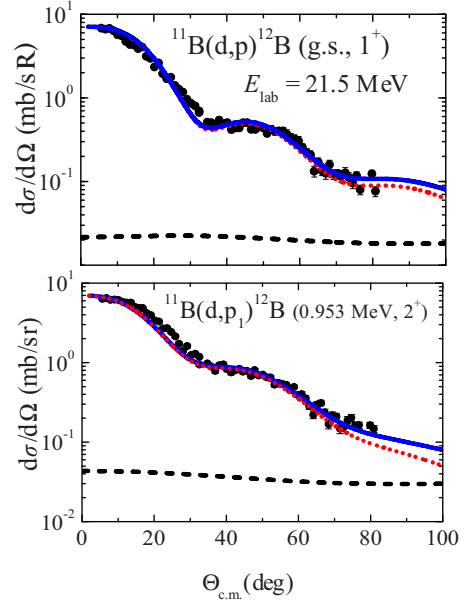
FIG. 3. Proton angular distributions from the ^{11}B$(d, p)^{12}$B reaction populated the 1^+ ground state and the first excited 0.95-MeV 2^+ state of ^{12}B at $E_d = 21.5$ MeV (points). The curves corresponds to the CRC (dotted lines) and CN (dashed lines) calculations, and their incoherent sum (solid lines).

scattering and reaction coupling effect. The final sets of parameters (see Table I) correspond to the best fit of the elastic-scattering data obtained. Parameters of the OPs describing the $p + {}^{12}$B interaction at 17–21 MeV and the $p + {}^{11}$B interaction at half of the proton energy are calculated based on the global parametrization presented in Ref. [41] and taking into account
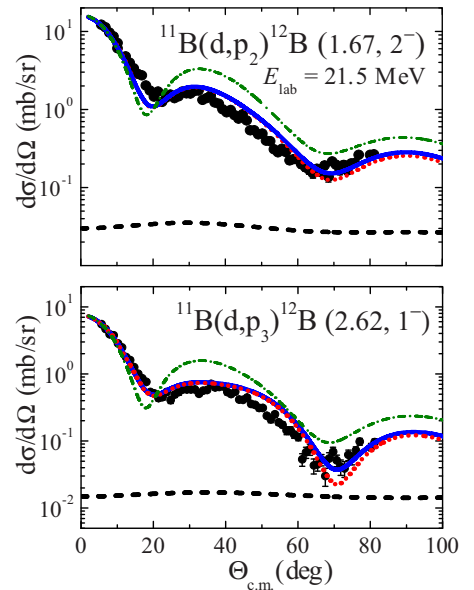
FIG. 4. The same as in Fig. 3, but for the second excited 1.67-MeV 2^- state and the third excited 2.62-MeV 1^- state of ^{12}B. The dash-dotted lines correspond to the CRC calculations with the standard geometric parameters $r_0 = 1.35$ fm and $a_0 = 0.65$ fm.
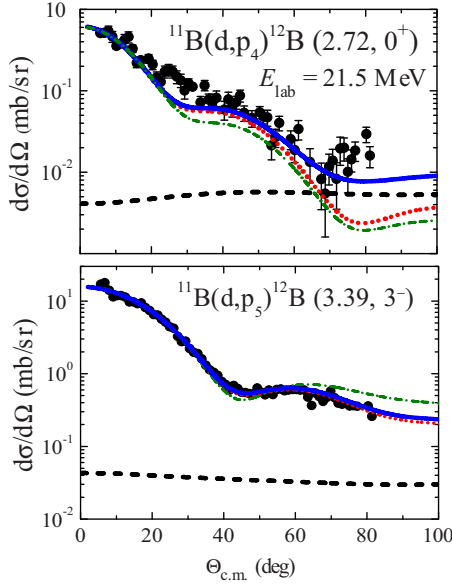
FIG. 5. The same as in Fig. 3, but for the fourth excited 2.72-MeV 0^+ state and the fifth excited 3.39-MeV 3^- state of ^{12}B. The dash-dotted lines correspond to the CRC calculations with the standard geometric parameters $r_0 = 1.35$ fm and $a_0 = 0.65$ fm.

corresponding energy dependence of the parameters V_0, W_D, r_0, r_{W_D}, and $r_{s.o.}$.

Figure 2 shows the angular distribution of deuterons scattered from ^{11}B at a deuteron laboratory energy of 21.5 MeV. The result of the CRC elastic-scattering calculation (solid line) is depicted in comparison with the measured data (circles). Parameters of the OPs presented in Table I are used for the reaction cross section calculations in the CRC and CN models.

B. Compound-nucleus analysis

The Hauser-Feshbach formalism of the statistical CN model is applied to carry out the compound-nucleus analysis of the ^{11}B(d, p) ^{12}B reaction. The results obtained with the code CNCOR [42] are shown in Figs. 3–5 (dashed lines) in comparison with the experimental differential cross sections. For the total width calculations, we take into account the decay into three main channels (p, n, and d) with the contribution from the levels located in the discreet (about 20–30 levels) and continuum spectra. The continuum spectrum contribution is calculated with standard parameters: the density level parameter $a = A/6.52$, the paring energy parameter $D = 1.509$, and the yrast-line-cutoff coefficient $y = 0.157$.

The analysis showed that the CN mechanism provides less than 1% of the cross section values at forward angles and manifests itself only at medium angles $\Theta_{c.m.} > 60°$ in the minima of the cross sections. This result supports a conjecture about a predominate role of the transfer mechanisms in this reaction at given energy.

C. Coupled-reaction-channels analysis

We performed CRC calculations of the ^{11}B(d, p) ^{12}B reaction, implying a finite-range one-neutron direct transfer mechanism, by using the code FRESCO [43]. The CRC method includes couplings between elastic scattering and direct transfer, thus bringing the calculations into agreement with the data.

The one-neutron direct transfer mechanism in the post representation relies on the interaction potential $V_{np} + U_{p+^{11}B} - U_{p+^{12}B}$, where V_{np} is the deuteron binding potential and the full complex remnant term $U_{p+^{11}B} - U_{p+^{12}B}$ represents the effective interactions (optical potentials, here) for the $p + {}^{11}$B and $p + {}^{12}$B channels. The distorted-wave Born approximation (DWBA) amplitude of the ^{11}B(d, p) ^{12}B reaction corresponds to the direct stripping mechanism ^{2}H$(I_d) + {}^{11}$B$(I_A) \rightarrow [p(s_p) + n(s_n)] + {}^{11}B(I_A) \rightarrow p(s_p) + {}^{12}B(I_f)$. We use a two-body potential model, where the exact overlap function is approximated by the model single-particle (sp) wave function, the radial part $\varphi_{An,lj}(r)$ of which is found as the eigenfunction of a core-neutron interaction potential $V_{An}(r)$ corresponding to the eigenvalue of the binding energy ε_{An}.

The proton-neutron sp overlap wave function in the deuteron, $\varphi_{pn,l=0, j=1/2}(r)$, with orbital angular momentum $l = 0$ (we suppose that the d-wave part of the deuteron wave function can be neglected in the cross-section calculations) is generated by the proton-neutron potential of a Gaussian form, $V_{pn}(r) = -72.15 \exp[-(r/1.484)^2]$ MeV with the ANC $C_{pn,l=0, j=1/2} = 0.87$ fm$^{-1/2}$ and the SF $S_{pn} = 1$.

For each state of ^{12}B we use the Woods-Saxon potentials $V_{^{11}Bn}(r)$ with varying radii and diffuseness parameters, the strengths of which are adjusted to fit the neutron binding energy in given state. The normalized sp overlap ^{11}B $+ n$ wave function $\varphi_{^{11}Bn,n_rlj}(r)$ generated by the $V_{^{11}Bn}(r)$ potential describes the relative motion of a core ^{11}B and a valence neutron in the specific state of ^{12}B characterized by the principle quantum number n_r, orbital l_2, and total j_2 angular momenta, which satisfy the angular-momentum coupling scheme (see, e.g., [21])

$$\mathbf{j_1} = \mathbf{s}_n + \mathbf{l_1}, \quad \mathbf{I}_d = \mathbf{j_1} + \mathbf{s}_p,$$
$$\mathbf{j_2} = \mathbf{s}_n + \mathbf{l_2}, \quad \mathbf{I}_f = \mathbf{j_2} + \mathbf{I}_A,$$
$$\mathbf{L} = \mathbf{j_1} + \mathbf{j_2} = \mathbf{l_1} + \mathbf{l_2}. \tag{3}$$

Here L is the transferred angular momentum, and l_1 and l_2 are the orbital angular momenta of the neutrons in the deuteron and ^{12}B, respectively; j_1 and j_2 are the total neutron angular momenta in the deuteron and ^{12}B. The quantum numbers of the last neutron in the ground and excited states of ^{12}B are shown in Table II.

Optimal sets of the geometric parameters of the ^{11}B $+ n$ interaction potentials giving the best fit to the data for different states are shown in Table II. CRC transfer calculations (dotted lines) are shown in Figs. 3–5. The solid curves represent the incoherent sum of the cross sections calculated in the CN and CRC models. The figures show that the calculations reproduce the proton angular distributions very well.

TABLE I. Parameters of the optical model potentials for the elastic scattering and ^{11}B(d, p_0)^{12}B reaction calculations.

Channel	V_0 (MeV)	r_0 (fm)	a_0 (fm)	W (MeV)	r_W (fm)	a_W (fm)	W_D (MeV fm)	r_{W_D} (fm)	a_{W_D} (fm)	$V_{s.o.}$ (fm)	$r_{s.o.}$ (fm)	$a_{s.o.}$ (fm)	r_C (fm)
$d +$^{11}B	80.8	1.180	0.75	0.4	1.35	0.63	8.0	1.30	0.85	6.0	1.05	1.10	1.3
$p +$^{12}B	55.0	1.125	0.57	0.			6.5	1.125	0.5	5.5	1.125	1.05	1.125
$p +$^{11}B	53.0	1.123	0.57	0.			6.6	1.123	0.5	5.5	1.123	1.05	1.123

The phenomenological or experimental SFs $S_{\rm expt}$ are determined as a ratio of the observed cross section to that calculated by an appropriate theoretical method. Their values are usually compared with theoretical SFs $S_{\rm th}$, which by a general definition (see, e.g., Refs. [21–23]) are the square norm of the overlap function of two cluster configurations. In the framework of a cluster approach, the overlap function is a model-independent characteristic of a nucleus and gives a probability of the total wave function of the nucleus to be composed of the wave functions of two clusters. The overlap function is not an eigenfunction of the Hermitian Hamiltonian and is not normalized to unity. Phenomenological SFs are also relative and are not normalized to unity. Theoretical SFs were introduced in the shell-model formalism and, for the nucleon transfer reactions, measure a degree of single-particle occupancy of a state [21–23]. Thus according to the halo criterion [11–15] mentioned above, halo candidates are expected to have large spectroscopic factors.

The structure of the low-lying levels of ^{12}B is usually considered in terms of the shell model and corresponds to the one-particle–one-hole shell-model configurations [30,31] exhibiting a very low degree of fragmentation of the sp strength. Thus the last neutron occupies the $1p$ orbital in the ground state, the 2^+ state, and the 0^+ state of ^{12}B. For other studied states of ^{12}B, the last neutron is localized in the $2s$ and $1d$ shells. The only shell-model orbital is available for the last neutron to form the 0^+ and 3^- states of ^{12}B: $1p_{1/2}$ and $1d_{5/2}$, respectively. It is reasonable to assume that a large probability of finding a neutron sp component in the total many-body wave function is connected with a high degree of peripherality of this neutron transfer reaction.

The transition amplitude for neutron transfer contains a coherent summation over the angular momenta j_1, l_1, j_2, l_2, L, and the interference between partial amplitudes can have a pronounced effect on the final cross sections. According to Table II, all transitions, such as to the ground state and to the excited states of ^{12}B as well (with the exception of the 2.72-MeV 0^+ state), are characterized by definite sets of the neutron angular momenta, that is why in Table II we show the amplitudes $\Theta_{l_2 j_2 I_f}^{^{12}{\rm B} \to ^{12}{\rm B}+n}$ of the SFs (the reduced widths) and also the SFs. The reduced widths are determined by comparing the experimental and model differential cross sections calculated with different $V_{^{11}{\rm B}n}$ potentials. Our calculations show that the ^{11}B $+ n$ wave functions do not depend on the

TABLE II. The excitation energies, spin-parities, neutron binding energies, geometric parameters of the ^{11}B $+ n$ interaction potential, sp quantum numbers (the principle quantum number, orbital, and total angular momenta), sp ANCs, reduced widths, and spectroscopic factors for the states of ^{12}B.

E_x (MeV)	J_f^π	ε_n (MeV)	r_0 (fm)	a (fm)	$n_2 l_2 j_2$			$b_{n_2 l_2}$ (fm$^{-1/2}$)	$\Theta_{n_2 l_2 j_2}^{\rm expt}$	$S_{n_2 l_2 j_2}^{\rm expt}$
0.0	1^+	3.37	1.35	0.65	1	1	1/2	1.37	0.37	0.14
					1	1	3/2		0.75	0.55
					1	1	1/2	1.03	0.23	0.05
							3/2	1.03	0.56	0.31
0.95	2^+	2.42	1.35	0.65	3	1	1/2	-1.45	0.42	0.18
							3/2	-1.45	0.05	0.0025
					3	3	5/2	0.10	0.05	0.0025
							7/2	0.10	0.0	0.0
1.67	2^-	1.69	1.85	0.80	2	0	1/2	-2.22	0.575	0.33
					2	2	3/2	0.43	0.115	0.013
					2	2	5/2	0.43	0.115	0.013
2.62	1^-	0.75	1.85	0.90	2	0	1/2	-1.32	0.79	0.63
					2	2	3/2	0.18	0.024	6×10^{-4}
					2	2	5/2	0.18	0.024	6×10^{-4}
2.72	0^+	0.65	1.75	0.65	1	1	3/2	0.45	0.34	0.113
3.39	3^-	0.01[a]	1.75	0.80	2	2	3/2	0.002	0.0	0.0
					2	2	5/2	0.002	0.50	0.25

[a]We use the effective positive binding energy of a valence neutron, whereas this state belongs to the continuum spectrum with $\varepsilon_n = -0.019$ MeV.

total spin j_2, because the interaction $^{11}\text{B} + n$ potential does not account for the spin-orbital interaction. In the result, the transfer amplitudes, which are characterized by two j_2 values complying with the angular-momentum coupling scheme (3) at the same $(n_2 l_2)$ subshell, are added incoherently, and the spectroscopic factors $S_{n_2 l_2}^{\text{expt}}$ for this subshell are calculated as the incoherent sum of squares of the reduced widths $\Theta_{n_2 l_2 j_2}^{\text{expt}}$. The experimental neutron SFs $S_{\text{expt}}(^{12}\text{B} \rightarrow {}^{11}\text{B} + n)$ for all states studied are shown in Tables II and III.

Note that parameters of the $^{11}\text{B} + n$ interaction potential generating the sp overlap $^{11}\text{B} + n$ wave function affect not only the SFs, but also the magnitudes and positions of maxima and minima of the proton angular distributions. As can be seen in Table II, in the g.s. and the 0.95-MeV 2^+ state, the geometric parameters have nearly standard values. However, those for the higher excited states have enlarged values (in comparison with the standard ones), $r_0 = 1.7\text{--}1.85$ fm and $a_0 = 0.80\text{--}0.95$ fm. Furthermore, the calculations with smaller geometric parameters fail to reproduce the shapes of the experimental proton angular distributions for these states. In Figs. 4 and 5, by way of illustrations, we show (by dashed-dotted lines) the cross sections of this reaction populating the 1.67-MeV 2^-, 2.62-MeV 1^-, 2.72-MeV 0^+, and 3.39-MeV 3^- states that are calculated with the standard geometric parameters $r_0 = 1.35$ fm and $a_0 = 0.65$ fm. One can see that the agreement of these calculations with the data is significantly worse. Using the enhanced geometric parameters in our calculations should not create confusion, because their increase, in general, characterizes an increase of the neutron-core interaction range and conforms with the enlarged radius of the neutron wave function in the higher excited states.

The 3.39-MeV 3^- state is situated in the continuum spectrum lying 0.019 MeV above the neutron-emission threshold. Nevertheless, in view of the small positive energy and the structure of the proton angular distribution being similar to those of the preceding bound states, we used the effective positive small (0.01 MeV) binding energy of the valence neutron.

The values of the neutron SFs and ANCs deduced via our CRC and CN analysis are shown in Table III in comparison with the results obtained by the DWBA analysis of the $^{11}\text{B}(d, p) {}^{12}\text{B}$ reaction in Refs. [17,44,45]. One can see that the SF for the 1^+ g.s. is in perfect agreement with the values reported earlier [44,45], as well as for the first excited 0.953-MeV 2^+ state when a sum over two possible $(n_2 l_2)$ orbitals is taken into account. For the higher excited states, the extracted $S_{n_2 l_2}^{\text{expt}}$ are found, in general, to be smaller in comparison with the previous results, which is related to the enlarged geometric parameters of the interaction sp potential that allowed us to reach a more detailed fit of the data. Note that the DWBA analyses performed in Ref. [44] were carried out in the zero-range approximation, assuming that only a single j_2 value of the transferred neutron contributes to each cross section. The DWBA calculations realized in Ref. [45] to describe the angular distribution data for the $^{11}\text{B}(d, p) {}^{12}\text{B}$ reaction in the inverse kinematics cover a very restricted angular interval $\theta_{\text{c.m.}} = 8°\text{--}28°$, where the uncertainty in the SF determination is rather large.

A decrease of the SFs for the 2.72-MeV 0^+ and the 3.39-MeV 3^- states (in comparison with the lower ones) indicates that a degree of the sp shell occupancy for the last neutron in these states is smaller than in the lower states.

III. ANC AND LAST NEUTRON RMS RADIUS CALCULATIONS

Neutron-transfer reactions with light nuclei are mainly peripheral; that is, they are actually sensitive only to the surface part of the neutron-core potential. Numerous studies have shown (see, e.g., Refs. [19–21] and references therein) that for the peripheral direct nuclear reactions the combination $S_{lj}^{\text{expt}}(\text{B} \rightarrow A + v) b_{Av,lj}^2$, which can be found from an appropriate theoretical analysis of the data, is almost constant or only weakly depends on the model parameters, contrary to the behavior of S_{lj}^{expt} and the sp ANC $b_{Av,lj}$ separately, which are obviously model dependent. Following Ref. [19], let us define the model-independent ANC as the product of a square-root of the SF $S(\text{B} \rightarrow A + n)$ (the reduced width $\Theta_{l_2 j_2 I_f}^{\text{B} \rightarrow A+n}$) and the sp ANC $b_{An,lj}$

$$C_{An,l_2 j_2 I_f} = \Theta_{l_2 j_2 I_f}^{\text{B} \rightarrow A+n} b_{An,l_2 j_2 I_f}. \tag{4}$$

Calculations of the ANCs accordingly to Eq. (4) with different sp wave functions enable us to answer the question of whether there exist states in ^{12}B that are formed due to the peripheral neutron transfer reactions. We can assume that the $^{11}\text{B}(d, p) {}^{12}\text{B}$ reaction at $E_{\text{lab}} = 21.5$ MeV, populating all studied states of ^{11}B, exhibits well the features of a peripheral process. A criterion of peripherality of this reaction is the persistence of $C_{An,lj}^{\text{expt}}$ in a number of cross-section calculations with different sp wave functions. The extracted ANC values shown in Table III differ from their averaged values no more than by 5% under reasonable changes of the sp potential parameters; i.e., the peripherality criterion is rather well fulfilled.

The ANC values found in our analysis are shown in Table III. For the 1^+ g.s., 1.67-MeV 2^-, and 2.62-MeV 1^- states they agree well within the error bars with those reported by Liu *et al.* [17]. Additionally, we deduced ANCs for the 0.95-MeV 2^+ and 2.72-MeV 0^+ states of ^{12}B.

It was already mentioned that, in the sp approximation, the exact overlap function is approximated by the two-body sp wave function. Thus the rms neutron radius R_n is approximately determined by the rms radius $\sqrt{\langle r^2 \rangle}$ of the sp neutron wave function (see, for instance, Eq. (13) in Ref. [24]). Samples of the sp overlap neutron wave functions $\varphi_{n_2 l_2 j_2}(r)$ for all studied states of ^{12}B are presented in Figs. 6 and 7 in comparison with the asymptotic parts of the corresponding Hankel functions $i k_{^{11}\text{B}n} h_l(i k_{^{11}\text{B}n} r)$. The sp functions $\varphi_{^{11}\text{B}n}(r)$ are multiplied by $(S_{n_2 l_2}^{\text{expt}})^{1/2}$ and the Hankel functions are multiplied by $C_{^{11}\text{B}n}^{\text{expt}}$. Figures 6 and 7 illustrate the coincidence of the asymptotic behavior of the sp and Hankel functions beyond $R_N \approx 5$ fm for all states except the 1^- state, for which $R_N \approx 5.5$ fm.

In accordance with a rigorous definition of a halo, it is assumed that the halo nucleon would spend about 50% of the time outside the range of the core potential [11–15,46]. This

TABLE III. Summary of the neutron spectroscopic factors, asymptotic normalization coefficients, rms neutron radii, and D_1 and D_2 coefficients for the states of ^{12}B.

E_x (MeV)	J_f^π	$n_2 l_2$	$S_{n_2 l_2}^{\text{expt}}$	$C_{^{11}\text{B}n}^{\text{expt}}$ (fm$^{-1/2}$)	$\left(C_{^{11}\text{B}n}^{\text{expt}}\right)^2$ (fm^{-1})	R_n (fm)	D_1 %	D_2 %	Ref.
0.0	1^+	1 1		1.16 ± 0.10	1.35 ± 0.23	3.16 ± 0.32	19.9	70.2	[17]
			0.69						[44,45]
			0.69	1.15 ± 0.06	1.31 ± 0.13	3.55 ± 0.20	11	57	this work
0.95	2^+	1 1	0.55/0.56						[44,45]
		1 1	0.36	0.62 ± 0.03	0.38 ± 0.04	3.8 ± 0.2	14	64	this work
		3 1	0.18	-0.62 ± 0.03	0.38 ± 0.04	4.5 ± 0.2	27	77	
1.67	2^-			1.34 ± 0.12	1.80 ± 0.43	4.01 ± 0.61	53.6	91.9	[17]
			0.57						[44,45]
		2 0	0.33	-1.28 ± 0.06	1.63 ± 0.16	$\mathbf{5.9 \pm 0.3}$	**53**	**94.5**	this work
		2 2	0.026	0.07	0.005	4.7 ± 0.2	28	77	
2.62	1^-			0.94 ± 0.08	0.88 ± 0.15	5.64 ± 0.90	66.8	96.3	[17]
		2 0	0.75						[44,45]
		2 0	0.63	-1.05 ± 0.05	1.10 ± 0.10	$\mathbf{7.4 \pm 0.4}$	**62**	**95.6**	this work
2.72	0^+	1 1	0.21						[44,45]
		1 1	0.113	0.15 ± 0.01	0.023 ± 0.002	$\mathbf{5.5 \pm 0.3}$	**37**	**86**	this work
3.39	3^-		0.5						[44,45]
		2 2	0.25			$\mathbf{5.9 \pm 0.3}$	**39**	**87**	this work

is a sufficiently strict requirement, whereas there are many "real halos" that are large, but have up to 50% of the neutron wave function remaining within the potential well [14]. Also, less developed halos and halo-like states do not exactly fulfill this criterion. To calculate this probability quantitatively, a coefficient $D_1(R_N)$ estimating the weight of the asymptotic part of the wave function is introduced,

$$D_1(R_N) = \frac{\int_{R_N}^\infty \varphi_{An,lj}^2(r) r^2 dr}{\int_0^\infty \varphi_{An,lj}^2(r) r^2 dr}$$
$$= \int_{R_N}^\infty \varphi_{An,lj}^2(r) r^2 dr, \qquad (5)$$
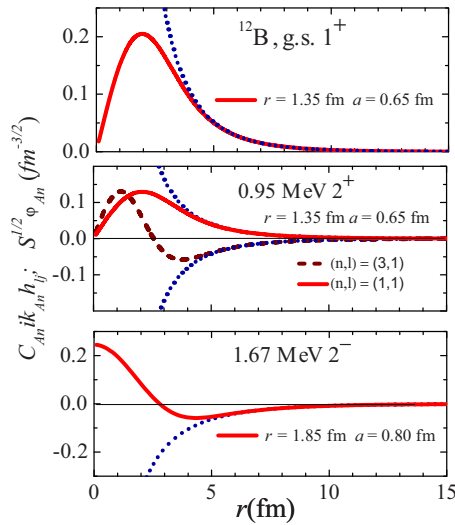
FIG. 6. Examples of the radial sp neutron wave functions $\varphi_{n_2 l_2}(r)$ multiplied by $(S^{\text{expt}})^{1/2}$ for the 1^+ g.s., the first excited 0.95-MeV 2^+ state, and the second excited 1.67-MeV 2^+ state of ^{12}B (solid and dashed lines) in comparison with the asymptotic parts of the corresponding Hankel functions $ik_{^{11}\text{B}n}h_l(ik_{^{11}\text{B}n}r)$ multiplied by $C_{^{11}\text{B}n}^{\text{expt}}$ (dotted lines).
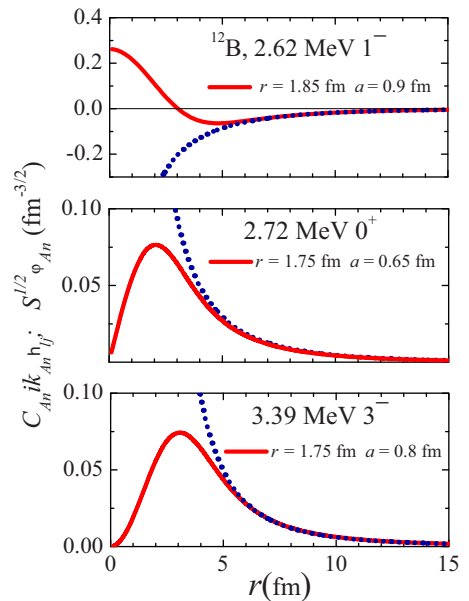
FIG. 7. The same as in Fig. 6, but for the third excited 2.62-MeV 1^- state, the fourth excited 2.72-MeV 0^+ state, and the fifth excited 3.39-MeV 3^- state of ^{12}B.

as well as a coefficient $D_2(R_N)$ estimating the contribution of the asymptotic part of the wave function to the rms radius,

$$
D_2(R_N) = \left(\frac{\int_{R_N}^{\infty} r^4 \varphi_{An,lj}^2(r) dr}{\int_0^{\infty} r^4 \varphi_{An,lj}^2(r) dr} \right)^{1/2}
$$
$$
= \left(\int_{R_N}^{\infty} r^4 \varphi_{An,lj}^2(r) dr \right)^{1/2} \Big/ R_n. \qquad (6)
$$

The main problem appearing here is a correct definition of the channel radius R_N. We will associate R_N with the distance where the sp neutron wave function gets out to the asymptotic region and coincides with the Hankel function. Then in the g.s. and all excited states, the channel radius R_N is 5 fm, with exception of the 2.62-MeV 1^-, for which $R_N = 5.5$ fm is used.

IV. DISCUSSION

Let us discuss the results presented in Table III.

Our calculations show that the rms radii of the last neutron in all excited states under consideration are greater than that in the g.s. of ^{12}B. Specifically, in the 2.62-MeV 1^- state, the radius is more than two times greater than the rms neutron radius in the g.s. The large values of D_1 and D_2 coefficients, 62% and 96%, respectively, determined for this state, along with the enormous neutron rms radius, $R_n(1^-) = 7.4 \pm 0.4$ fm, undoubtedly indicate that the 2.62-MeV 1^- state possesses a neutron halo with the halo radius $R_h(1^-) = R_n(1^-)$.

The 1.67-MeV 2^- state evidently can also be considered as the halo state, with the last neutron spending more than 50% of its time outside the range of the core potential and the neutron rms radius $R_n(2^-) = R_h(2^-) = 5.9 \pm 0.3$ fm, which exceeds that for the g.s. by a factor of 1.7. This result confirms a conclusion made by Liu and collaborators in Ref. [17] that the second (1.67-MeV 2^-) and third (2.62-MeV 1^-) excited states of ^{12}B are the neutron halo states. Nevertheless, our analysis indicated that the halo radii in these states are considerably greater.

In the 2.72-MeV 0^+ state located 0.65 MeV below the neutron-emission threshold, the neutron rms radius is also found to be enlarged, but is smaller than that in the 1.67-MeV 2^- state, $R_n(0^+) = 5.5 \pm 0.3$ fm, and $D_2 = 86\%$. One can see that $D_1 = 37\%$ is less than 50% and the SF $S_{n_2l_2}^{\text{expt}} = 0.113$ is reduced in comparison with the lower states. We propose the 2.72-MeV 0^+ state as a neutron halo-like state, in which the halo features are beginning to appear and manifest themselves in the enlarged neutron rms radius.

The most interesting case is concerned with the 3.39-MeV 3^- excited state localized only 0.019 MeV above the neutron-emission threshold. Since this state belongs to the continuum spectrum, there is no way to correctly calculate its ANC. In order to determine the radius of ^{12}B in this state, we carried out the calculation with a very small positive neutron binding energy ($\varepsilon = -0.01$ MeV) and found that the asymptotic behavior of the sp and Hankel functions becomes the same at the distance about 5.0 fm. Thus, we can determine the rms radius of the last neutron by determining the rms radius of the sp wave function. It is found to be $R_n = 5.9$ fm, which is equal to the neutron rms radius in the 1.67-MeV 2^- state of ^{12}B and is a factor of 1.7 greater than that for the g.s. The

contribution of the asymptotic part of the wave function to the rms radius, the D_2 coefficient, achieves 87% compared with 92% for the 1.67-MeV 2^- state. The neutron transfer reaction to this state is definitely peripheral, though the weight of the asymptotic part of the neutron wave function, D_1, is lower than 50%, $D_1 = 39\%$, and the extracted phenomenological SF $S_{n_2l_2}^{\text{expt}} = 0.25$. Thus we propose that the 3.39-MeV 3^- excited state in ^{12}B is a neutron halo-like state with enhanced neutron radius $R_n = 5.9 \pm 0.3$ fm and the orbital momentum $l_n = 2$ of the last neutron.

Our results confirm the statement above that the halo phenomenon has a universal character and appears as in the ground states of exotic nuclei and in the excited states of normal light nuclei. The enlarged radii obtained in our work, as well as the respective D_1 and D_2 coefficients are emphasized in Table III by bold.

Table IV shows the summary of the neutron halo radii R_h in the excited states accordingly to the recent data obtained by different methods, the neutron orbital momenta l_n, and the neutron binding energies ε_n. The rms radii of nucleus R_{rms} in the given state is also shown. A relationship between the one-neutron halo radius R_h and the rms radii R_{rms} of the core-nucleus A and the $(A + 1)$ system proposed by Tostevin and Al-Khalili in Ref. [47],

$$
(A + 1)[R_{\text{rms}}(A + 1)]^2 = A[R_{\text{rms}}(A)]^2 + [A/(A + 1)]R_h^2,
$$
$$
(7)
$$

is used to relate these radii. The rms matter radii of ^{10}Be, ^{11}B, ^{12}C, and ^{13}C are taken to be 2.30, 2.09, 2.35, and 2.28 fm, respectively, from Ref. [48].

The halo states are characterized not only by the extent radius of valence neutrons, but also by the enhanced matter radius of a nucleus itself. This fact is definitely seen from Table IV, where the halo radii (the last neutron rms radii) and the rms matter radii of the corresponding nuclei in the excited states are shown. Note that the rms matter radii of ^{9}Be, ^{12}B, ^{13}C, and ^{14}C in the ground states are adopted as 2.38, 2.39, 2.28, and 2.30 fm, respectively [48].

The existence of neutron halos in the short-lived excited states of some stable and radioactive nuclei was revealed, in particular, by the ANC analysis of the neutron-transfer reactions [17,24,51]. Liu *et al.* [17] reported the observation of halos in the first ($1/2^+$, $E_x = 3.089$ MeV) excited state of ^{13}C and the second (2^-, $E_x = 1.674$ MeV) and the third (1^-, $E_x = 2.621$ MeV) excited states of ^{12}B in the (d, p) reactions on ^{12}C and ^{11}B, respectively. The (d, p) reaction analysis made in Ref. [51] showed that neutron halos exist in the first 1^- and 0^- excited states of the radioactive carbon isotope ^{14}C. We have shown in Ref. [24] that ^{11}Be possesses one neuron halo not only in the $1/2^+$ g.s. (with the halo radius $R_h = 8.0 \pm 0.2$ fm), but in the first excited 0.32-MeV $1/2^-$ state as well (with the halo radius $R_h = 4.65 \pm 0.20$ fm). The much smaller halo radius for the first excited state in comparison with the g.s. is a consequence of the fact that the valence neutron has an orbital moment $l = 1$.

A neutron halo in the 1.68-MeV $1/2_1^+$ state of ^{9}Be, located 15 keV above the neutron emission threshold, was recently found by MDM analysis of the $\alpha + {}^9$Be inelastic scattering

TABLE IV. Summary of the rms matter radii and halo radii in the excited states of light nuclei.

Nucleus	J_f^π, E_x (MeV)	$R_{\rm rms}$ (fm)	$R_{\rm h}$ (fm)	l_n	ε_n (MeV)	Method
^{9}Be	$1/2^+$, 1.68	3.42 ± 0.20	8.2^a	1	-0.015	MDM, [16]
^{11}Be	$1/2^-$, 0.32	2.57 ± 0.05	4.65 ± 0.20	1	0.18	ANC, [24]
^{12}B	2^-, 1.67	2.29 ± 0.24	4.01 ± 0.61	0	1.69	ANC, [17]
		2.58 ± 0.11	5.90 ± 0.30			ANC, this work
	1^-, 2.62	2.54 ± 0.33	5.64 ± 0.90	0	0.75	ANC, [17]
		2.86 ± 0.11	7.40 ± 0.35			ANC, this work
	0^+, 2.72^b	2.51 ± 0.11	5.48 ± 0.30	1	0.65	ANC, this work
	3^-, 3.39^b	2.58 ± 0.11	5.90 ± 0.30	2	-0.019	ANC, this work
^{13}C	$1/2^+$, 3.09	2.40 ± 0.15	5.04 ± 0.75			ANC, [17]
		2.72 ± 0.10	5.72 ± 0.16	0	1.86	ANC, [24]
		2.74 ± 0.06	5.88 ± 0.40^a			MDM, [49]
		2.68	5.47			OCM, [50]
^{14}C	1^-, 6.09	2.49 ± 0.11	4.57 ± 0.30	0	2.08	ANC, [51]
	1^-, 6.90	2.65 ± 0.12	5.78 ± 0.36	0	1.27	ANC, [51]

$^a R_{\rm h}$ is calculated from the corresponding $R_{\rm rms}$ value by Eq. (7).
^{b}The halo-like state.

at various energies [16,52,53]. The halo structure observed in this state is formed by a valence neutron occupying the p orbital, similar to that observed in the first excited state of ^{11}Be. The ^{9}Be nucleus in the 3.053-MeV $5/2^+$ and 4.70-MeV $3/2^+$ states and ^{11}Be in the 1.78-MeV $5/2^+$ and 3.41-MeV $3/2^+$ states provide other very possible candidates to possess neutron halos in the unbound states [49,53].

Table IV shows that the neutron halos in the excited states of light nuclei possess the same properties as neutron halos in the ground states of exotic radioactive nuclei: (1) location of the corresponding states below neutron emission thresholds and close to them, and (2) occupation of the s orbital by the valence neutron. In addition, halos in the excited states have new properties: (3) existence of halos as in the discrete and in the continuum spectra as well, and (4) possession also of the nonzero orbital momenta $l_n = 1$ and 2.

Exotic states of light nuclei are not limited by the neutron-halo structures. Very recently the observation of a proton halo in the unbound 2.37-MeV $1/2^+$ state of ^{13}N, a mirror state with respect to the 3.09-MeV state of ^{13}C, was reported [37]. The enhanced rms radius of ^{13}N in this state (in comparison with the g.s. radius equal to 2.31 fm) was found to be equal to 2.91 ± 0.14 fm. This value is closed to the radius of ^{13}C in the mirror 3.09 MeV state (its estimates ranges from 2.7 to 2.9 fm, as shown, for instance, in Ref. [24]).

V. CONCLUSIONS

In recent years a considerable amount of research has been realized on neutron- and proton-transfer reactions, both in the traditional kinematics with stable and radioactive beams on light targets and in the inverse kinematics, especially with radioactive targets. The obtained data contain relevant astrophysical and spectroscopic information about neutron and proton single-particle states of nuclei. Many of these reactions are proved to have a peripheral character and can be used for extracting the ANCs and estimating the last neutron and proton radii, including radii of nuclei in the short-lived

excited states. In our paper, we measured the differential cross sections of the ^{11}B(d, p) ^{12}B reaction at $E_d = 21.5$ MeV populating the 1^+ ground state and the 0.95-MeV 2^+, 1.67-MeV 2^-, 2.62-MeV 1^-, 2.72-MeV 0^+, and 3.39-MeV 3^- excited states. The analysis of the data at $\theta_{\rm c.m.} \simeq 5°$–$85°$ was carried out within the coupled-reaction-channels method for the direct neutron transfer and the Hauser-Feshbach formalism of the statistical compound-nucleus model. The spectroscopic factors, asymptotic normalization coefficients, and rms radii of the last neutron in all states studied were deduced. The existence of neutron halos in the 1.67-MeV 2^- and 2.62-MeV 1^- states was found, consistent with the earlier published data. The large neutron rms radius (5.5 ± 0.3) was found for the 2.72-MeV 0^+ state located 0.65 MeV below the neutron-emission threshold. This state can be considered as a neutron halo-like state with the orbital momentum $l_n = 1$. New information was obtained about the enlarged rms radius (5.9 fm) of the last neutron in the unbound 3.39-MeV 3^- state of ^{12}B, which also can be identified as a neutron halo-like state with the orbital momentum $l_n = 2$ of the last neutron. Estimates of the matter radii of nuclei possessing halo states revealed their enhanced sizes as well.

The results presented in this paper for the radii of ^{12}B in the halo states can be useful for determining the radii of the nuclei with $A = 12$ by other methods, which, in particular, employ charge-exchange reactions to the isobaric analog states located above the nucleon-emission threshold.

[1] I. Tanihata *et al.*, Phys. Lett. B **160**, 380 (1985).

[2] I. Tanihata, H. Hamagaki, O. Hashimoto, Y. Shida, N. Yoshikawa, K. Sugimoto, O. Yamakawa, T. Kobayashi, and N. Takahashi, Phys. Rev. Lett. **55**, 2676 (1985).

[3] K. Riisager, A. S. Jensen, and P. MØller, Nucl. Phys. A **548**, 393 (1992).

[4] P. G. Hansen, A. S. Jensen, and B. Jonson, Annu. Rev. Nucl. Part. Sci. **45**, 591 (1995).

[5] I. Tanihata, H. Savajols, and R. Kanungod, Prog. Part. Nucl. Phys. **68**, 215 (2013).

[6] Z.-T. Lu, P. Mueller, G. W. F. Drake, W. Nörtershäuser, Steven C. Pieper, and Z.-C. Yan, Rev. Mod. Phys. **85**, 1383 (2013).

[7] T. Otsuka, N. Fukunishi, and H. Sagawa, Phys. Rev. Lett. **70**, 1385 (1993).

[8] T. Otsuka, M. Ishihara, N. Fukunishi, T. Nakamura, and M. Yokoyama, Phys. Rev. C **49**, R2289 (1994).

[9] K. Riisager, Phys. Scr. **T152**, 014001 (2013).

[10] Shubhchintak, Phys. Rev. C **96**, 024615 (2017).

[11] K. Riisager, D. V. Fedorov, and A. S. Jensen, Europhys. Lett. **49**, 547 (2000).

[12] A. S. Jensen and M. V. Zhukov, Nucl. Phys. A **693**, 411 (2001).

[13] A. S. Jensen, K. Riisager, D. V. Fedorov, and E. Garrido, Rev. Mod. Phys. **76**, 215 (2004).

[14] K. Riisager, Rev. Mod. Phys. **66**, 1105 (1994).

[15] K. Riisager, *Nuclear Halos and Experiments to Probe Them*, Lecture Notes in Physics Vol. 700 (Springer, Berlin, 2006).

[16] A. A. Ogloblin, A. N. Danilov, A. S. Demyanova, S. A. Goncharov, T. L. Belyaeva, and W. Trzaska, in *Nuclear Particle Correlations and Cluster Physics* (World Scientific, Singapore, 2017), p. 311.

[17] Z. H. Liu, C. J. Lin, H. Q. Zhang, Z. C. Li, J. S. Zhang, Y. W. Wu, F. Yang, M. Ruan, J. C. Liu, S. Y. Li, and Z. H. Peng, Phys. Rev. C **64**, 034312 (2001).

[18] B. Guo, Z. H. Li, W. P. Liu, and X. X. Bai, J. Phys. G: Nucl. Part. Phys. **34**, 103 (2007).

[19] L. D. Blokhintsev, I. Borbely, and E. I. Dolinskii, Fiz. Elem. Chastits At. Yadra **8**, 1189 (1977) [Sov. J. Part. Nuclei **8**, 485 (1977)].

[20] S. A. Goncharov, J. Dobesh, E. I. Dolinsky, A. M. Mukhamedzhanov, and J. Cejpek, Yad. Fiz. **35**, 662 (1982) [Sov. J. Nucl. Phys. **35**, 383 (1982)].

[21] G. R. Satchler, *Direct Nuclear Reactions* (Clarendon, Oxford, 1983).

[22] N. K. Glendenning, *Direct Nuclear Reactions* (World Scientific, Singapore, 2004).

[23] A. M. Mukhamedzhanov and F. M. Nunes, Phys. Rev. C **72**, 017602 (2005).

[24] T. L. Belyaeva, R. Perez-Torres, A. A. Ogloblin, A. S. Demyanova, S. N. Ershov, and S. A. Goncharov, Phys. Rev. C **90**, 064610 (2014).

[25] D. Y. Pang and A. M. Mukhamedzhanov, Phys. Rev. C **90**, 044611 (2014).

[26] A. M. Mukhamedzhanov and D. Y. Pang, Phys. Rev. C **92**, 014625 (2015).

[27] Yu. V. Orlov, B. F. Irgaziev, and L. I. Nikitina, Phys. Rev. C **93**, 014612 (2016).

[28] Yu. V. Orlov, B. F. Irgaziev, and Jameel-Un Nabi, Phys. Rev. C **96**, 025809 (2017).

[29] A. Grassi, G. Mangano, L. E. Marcucci, and O. Pisanti, Phys. Rev. C **96**, 045807 (2017).

[30] F. Ajzenberg-Selove, Nucl. Phys. A **506**, 1 (1990).

[31] K. Peräjärvi, C. B. Fu, G. V. Rogachev, G. Chubarian, V. Z. Goldberg, F. Q. Guo, D. Lee, D. M. Moltz, J. Powell, B. B. Skorodumov, G. Tabacaru, X. D. Tang, R. E. Tribble, B. A. Brown, A. Volya, and J. Cerny, Phys. Rev. C **74**, 024306 (2006).

[32] N. K. Timofeyuk, R. C. Johnson, and A. M. Mukhamedzhanov, Phys. Rev. Lett. **91**, 232501 (2003).

[33] N. K. Timofeyuk and P. Descouvemont, Phys. Rev. C **71**, 064305 (2005).

[34] A. S. Demyanova, A. A. Ogloblin, S. A. Goncharov, and T. L. Belyaeva, Int. J. Mod. Phys. E **17**, 2118 (2008).

[35] A. S. Demyanova, T. L. Belyaeva, A. N. Danilov, Yu. A. Glukhov, S. A. Goncharov, S. V. Khlebnikov, V. A. Maslov, Yu. D. Molchalov, Yu. E. Penionzhkevich, R. V. Revenko, M. V. Safonenko, Yu. G. Sobolev, W. Traska, G. P. Tyurin, and A. A. Ogloblin, Phys. At. Nucl. **72**, 1611 (2009).

[36] A. N. Danilov, T. L. Belyaeva, A. S. Demyanova, S. A. Goncharov, and A. A. Ogloblin, Phys. Rev. C **80**, 054603 (2009).

[37] A. S. Demyanova, A. A. Ogloblin, A. N. Danilov, T. L. Belyaeva, S. A. Goncharov, and W. Trzaska, JETP Lett. **104**, 526 (2016); A. S. Demyanova, A. A. Ogloblin, S. A. Goncharov, A. N. Danilov, T. L. Belyaeva, and W. Trzaska, Yad. Fiz. **80**, 427 (2017) [Phys. At. Nucl. **80**, 831 (2017)].

[38] A. Danilov, A. Demyanova, A. Ogloblin, T. Belyaeva, S. Goncharov, R. Sukhorukov, V. Maslov, Y. Sobolev, W. Trzaska, S. Khlebnikov, G. Tyurin, N. Burtebaev, D. Janseitov, E. Mukhamejanov, and Y. Gurov, in *The 3rd International Conference on Particle Physics and Astrophysics*, 2–5 October 2017, Moscow, edited by Z. Pavel, I. Selyuzhenkov, and A Taranenko (KnE, Dubai, 2018), p. 83.

[39] H. An and Ch. Cai, Phys. Rev. C **73**, 054605 (2006).

[40] C. M. Perey and F. G. Perey, Phys. Rev. **132**, 755 (1963).

[41] B. A. Watson, P. P. Singh, and R. E. Segel, Phys. Rev. **182**, 977 (1969).

[42] T. L. Belyaeva, N. S. Zelenskaya, and N. V. Odintsov, Comput. Phys. Commun. **73**, 161 (1992).

[43] I. J. Thompson, FRESCO user's manual and code, available from the author.

[44] J. E. Monhan, H. T. Fortune, C. M. Vincent, and R. E. Segel, Phys. Rev. C **3**, 2192 (1971).

[45] H. Y. Lee, J. P. Greene, C. L. Jiang, R. C. Pardo, K. E. Rehm, J. P. Schiffer, A. H. Wuosmaa, N. J. Goodman, J. C. Lighthall, S. T. Marley, K. Otsuki, N. Patel, M. Beard, M. Notani, and X. D. Tang, Phys. Rev. C **81**, 015802 (2010).

[46] B. Jonson, Phys. Rep. **389**, 1 (2004).

[47] J. A. Tostevin and J. S. Al-Khalili, Nucl. Phys. A **616**, 418 (1997).

[48] A. Ozawa, T. Suzuki, and I. Tanihata, Nucl. Phys. A **693**, 32 (2001).

[49] A. A. Ogloblin, A. N. Danilov, T. L. Belyaeva, A. S. Demyanova, S. A. Goncharov, and W. Trzaska, Phys. Rev. C **84**, 054601 (2011); Yad. Fiz. **74**, 1581 (2011); [Phys. At. Nucl. **74**, 1548 (2011)].

[50] T. Yamada and Y. Funaki, Int. J. Mod. Phys. E **17**, 2101 (2008).

[51] Z. H. Liu, Chin. Phys. Lett. **19**, 1071 (2002).

[52] A. S. Demyanova *et al.*, EPJ Web Conf. **66**, 02026 (2014).

[53] A. S. Demyanova *et al.*, Pis'ma Zh. Eksp. Teor. Fiz. **102**, 467 (2015) [JETP Lett. **102**, 413 (2015)].